Feasibility of measuring nonanalytic QED coupling from pair creation in strong fields

B. King [1,*] and S. Tang [2,†]

[1] *Centre for Mathematical Sciences, University of Plymouth, Plymouth PL4 8AA, United Kingdom*

[2] *College of Physics and Optoelectronic Engineering, Ocean University of China, Qingdao, Shandong 266100, China*

(Received 10 January 2024; accepted 20 February 2024; published 28 March 2024)

In the quasistatic regimes of nonlinear Breit-Wheeler and trident pair creation, the rates can exhibit a nonanalytic dependency on the fundamental coupling of quantum electrodynamics, in a form similar to Schwinger vacuum pair creation. To reach this tunneling regime requires satisfying competing requirements: a high-intensity but low quantum strong-field parameter with sufficient pair creation to be observed. Using a locally monochromatic approach, we identify the parameter regime where tunneling pair creation could be measured in experiment. Studying several scenarios of collisions with focused Gaussian pulses, including a bremsstrahlung and an inverse Compton source for nonlinear Breit-Wheeler and a Gaussian electron beam for nonlinear trident, we find the position of the tunneling parameter regime to be well defined and robust.

DOI: 10.1103/PhysRevA.109.032823

I. INTRODUCTION

Electromagnetic (EM) fields can be converted into electron-positron pairs via a variety of mechanisms. It was predicted by Breit and Wheeler [1] that colliding two real photons with sufficient energy should allow their conversion to an electron-positron pair, and this was recently observed with quasireal photons in ultraperipheral collisions of heavy ions at ATLAS [2,3] and CMS [4]. Alternatively, photons can be converted to electron-positron pairs in the Coulomb fields of nuclei via the Bethe-Heitler process [5]. These are examples of *linear*, leading-order perturbative processes. In contrast, *nonlinear* Breit-Wheeler [6–11] involves higher numbers of photons, which can occur when a photon scatters in a coherent field where the center-of-mass energy is too low for the linear, two-photon process, to proceed. Nonlinear Breit-Wheeler was observed in the *multiphoton* regime in the landmark E144 experiment [12,13] as the second part of the nonlinear trident process, in which an electron that collides with an EM pulse emits a photon via nonlinear Compton scattering which subsequently is converted to an electron-positron pair. The LUXE experiment [14] at DESY and the E320 experiment [15] at SLAC plan to employ intense laser pulses to observe nonlinear Breit-Wheeler in the all-order regime where arbitrarily high numbers of photons are involved in the creation of a pair. This regime is often referred to as "nonperturbative" because the coupling of the laser photons to the pair is given by the intensity parameter, ξ, which can nowadays routinely exceed unity in experiments [16] and so including the interaction perturbatively is no longer accurate. The laser photon coupling can be related to the elementary QED coupling with $\xi^2 = 4\pi\alpha_{\mathsf{qed}}\lambda\!\!\!^{-2}_{\mathsf{c}}\lambda\!\!\!^{-}n_l$, where $\alpha_{\mathsf{qed}} = e^2/4\pi\hbar c$, $e > 0$ is the charge of a positron, n_l is the number density of laser photons of wavelength λ in the background, $\lambda\!\!\!^{-}_{\mathsf{c}} = \hbar/mc$ the reduced Compton wavelength, and $\lambda\!\!\!^{-} = \lambda/2\pi$ [17]. Although $\alpha_{\mathsf{qed}} \ll 1$, as the *density* of photons increases, the $\xi \gtrsim O(1)$ regime is accessible. We note that the $\hbar$ dependency in α_{qed} and n_l cancels with the $\hbar$ dependency of $\lambda\!\!\!^{-2}_{\mathsf{c}}$; ξ is of classical origin. This "nonperturbativity at small coupling" has analogies with other fields, such as gluon saturation in inelastic scattering [18,19].

The pair creation process referred to as Schwinger pair creation [20], which was already conceived by Sauter [21] and calculated by Heisenberg and Euler [22], is often contrasted to the Breit-Wheeler process since it traditionally considers pairs produced directly from a constant or slowly varying electric field. However, more realistic scenarios for observing this process in experiment involve "assisting" Schwinger [23–34] by adding a high-frequency but low-intensity field. Therefore, we might expect that in some parameter regime there is similarity to nonlinear Breit-Wheeler which considers a slowly varying background (albeit one that can be well approximated as a plane wave) colliding with a high-energy (frequency) photon. (Recently scenarios have also been considered where nonlinear Breit-Wheeler is "assisted" by a combination of low- and high-frequency laser pulse [35–38].) Schwinger pair creation is often highlighted as special, because of the nonanalytic dependency on the QED coupling, α_{qed}, in a constant electric field. This is a second type of nonperturbativity; unlike the small-coupling case, which is an entirely classical effect, the nonanalytic dependence on α_{qed} is a fundamentally quantum nonperturbativity. Therefore it is of interest to observe this type of nonperturbativity as an aim separate to the classical "small-coupling" nonperturbativity when $\xi \gtrsim O(1)$.

It is known that the nonlinear Breit-Wheeler process, just like the Schwinger process, can exhibit a nonanalytic dependency on α_{qed} in the "quasistatic" or "locally constant" regime. In nonlinear Breit-Wheeler, a key quantity is the strong-field parameter, χ, which for a charge in a plane wave background is exactly $\chi = E_{\mathsf{r.f}}/E_{\mathsf{qed}}$, i.e., the ratio of the field strength in the charge's rest frame, $E_{\mathsf{r.f}}$, to the QED field strength scale ("Schwinger limit"), $E_{\mathsf{qed}} = m^2c^3/e\hbar$. Since $\chi \propto \hbar$, we see it is a quantum parameter and therefore cannot be acquired from ξ. The QED coupling then appears in the

*b.king@plymouth.ac.uk

†tangsuo@ouc.edu.cn

nonlinear Breit-Wheeler rate, in the square root of the denominator of an exponent, just as in the Schwinger process. We will refer to this as the *tunneling regime* for simplicity (even though the potential is a plane wave and not static). It was suggested in [39,40] to measure nonlinear Breit-Wheeler in the tunneling regime by combining a bremsstrahlung photon source with a monochromatic laser and vary its intensity. However, to reach the tunneling regime with a fixed photon energy, opposing limits must be fulfilled, $\xi \gg 1$ and $\chi \ll 1$, while also producing sufficient pairs to be measurable. Furthermore, the tunneling regime is an *asymptotic* limit and so it is unclear before calculation what the magnitude of parameters must be for the process to be well described by this regime.

In the current paper, we outline the limited but accessible parameter space in which experiments could observe the nonanalytic dependency on α_{qed} in nonlinear pair creation. This region crucially depends on photon energy as well as EM field intensity and is reachable at high-intensity laser facilities [41–43] as well as at laser-particle experiments LUXE [14,44] and E320 [15]. We cannot use the standard locally constant field approximation (LCFA) to calculate the rate of strong-field QED processes because the tunneling regime is a limit of this approximation, and so a more accurate calculational framework that does not rely upon locally constant rates is required. For this reason, we employ in our analysis the locally monochromatic approximation [45] (LMA), which includes the fast timescale of the carrier frequency exactly, but the slow timescale of the pulse envelope perturbatively (through a local approximation). The LMA is a good approximation for all values of intensity parameter ξ and strong-field parameter χ when used to calculate the nonlinear Breit-Wheeler process in backgrounds that are "plane-wave-like," i.e., have a well-defined central frequency. The narrower the bandwidth of the background, the more accurate the LMA becomes. When benchmarked with exact but expensive QED calculations in a plane-wave pulse [46], the LMA was found to become less accurate: (1) in very short pulses and (2) when the energy parameter was at a value close to a multiphoton channel opening; subsequent analysis [47] revealed contributions from the pulse envelope become important in these cases. In the current paper, the interest is in the tunneling regime, which can be revealed when the background is modeled as locally constant, i.e., without a frequency parameter and hence neither (1) nor (2) of the aforementioned cases of discrepancy is relevant here. Indeed, to compare with the underlying theory, one would favour weakly focused, quasimonochromatic backgrounds, with wide focal spots; as a result the LMA has been incorporated into the open source Ptarmigan simulation code [48,49] and also used for higher-order processes such as trident [50]. We employ Ptarmigan's rate generator for pair creation, which allows efficient calculation of the LMA at high intensities. Our aim is to assess the feasibility of measuring pair creation in the tunneling regime, and to this end we consider scenarios that include probe beam distributions and focused laser backgrounds.

We organize the investigation by introducing increasingly detailed modeling of potential experiments in each successive section. This begins with the general situation in Sec. II, with monoenergetic photons colliding with a plane-wave background. In Sec. III the monoenergetic photons are replaced with a photon source from (1) an amorphous bremsstrahlung target and (2) inverse Compton-scattering, and the plane-wave background is replaced with a Gaussian focused laser pulse. In Sec. IV we investigate a scenario for measuring the nonanalytic coupling using an electron probe in the two-step nonlinear trident process. In Sec. V we conclude the feasibility study of measuring Schwinger-like pair creation using intense lasers. (Unless otherwise stated, we set $\hbar = c = 1$ throughout.)

II. MONOENERGETIC PHOTONS, PLANE-WAVE BACKGROUND

Here we consider monoenergetic photons colliding with a plane-wave background which demonstrates the essence of the problem. The tunneling rate, $\mathsf{P}_{\mathsf{tun}}$, for pair creation via nonlinear Breit-Wheeler is [51]

$$\frac{d\mathsf{P}_{\mathsf{asy}}}{d\varphi} = \frac{\alpha_{\mathsf{qed}}}{\eta}\frac{3}{16}\sqrt{\frac{3}{2}}\,\chi\,\exp\left[-\frac{8}{3\chi}\right], \tag{1}$$

where $\varphi = \varkappa \cdot x$ is the plane-wave phase and the energy parameter of the photon with momentum ℓ is $\eta = \varkappa \cdot \ell/m^2$. We compare this to the rate of pair creation via the Schwinger mechanism [52–54]:

$$\frac{d^4\mathsf{P}_{\mathsf{Sch.}}}{dx^4} = \frac{\alpha_{\mathsf{qed}}}{4\pi^2}\mathfrak{a}\mathfrak{b}\coth\left(\frac{\pi\mathfrak{b}}{\mathfrak{a}}\right)\exp\left[-\frac{\pi E_{\mathsf{qed}}}{\mathfrak{a}}\right], \tag{2}$$

where the secular field invariants are

$$\mathfrak{a},\mathfrak{b} = \left[\sqrt{\mathcal{S}^2+\mathcal{P}^2} \pm \mathcal{S}\right]^{1/2} \tag{3}$$

and $\mathcal{S} = -F_{\mu\nu}F^{\mu\nu}/4$ with $\mathcal{P} = -\widetilde{F}_{\mu\nu}F^{\mu\nu}/4$ are the standard EM invariants where F is the field tensor and $\widetilde{F}$ is its dual. We note the common nonanalytic dependency on the fundamental QED coupling of these rates since $1/\chi \propto 1/\sqrt{\alpha_{\mathsf{qed}}}$ in Eq. (1) and $E_{\mathsf{qed}} \propto 1/\sqrt{\alpha_{\mathsf{qed}}}$ in Eq. (2). (Breit-Wheeler is sometimes distinguished from Schwinger with the argument that $\mathcal{S}$ and $\mathcal{P}$ are zero in a plane wave background. and hence the contribution from the Schwinger process is zero. In Appendix A we note that when, in the definition of F, the photon is taken into account as well as the plane-wave background, $\mathcal{S}$ and $\mathcal{P}$ are clearly nonzero and in fact proportional to χ.)

The tunneling rate in Eq. (1) is the $\chi \to 0$ asymptotic limit of that in a locally constant EM background. The locally constant field approximation (LCFA) is expected to be a good approximation when $\xi \gg 1$ but for pair creation also requires that the photon energy parameter, η, is not too high [46] (otherwise pair creation can proceed via the multiphoton process, which is not captured by the LCFA). Therefore for the tunneling rate in Eq. (1) to be accurate, we have two limits: (1) $\xi \to \infty$ for the LCFA to be accurate and (2) $\chi \to 0$ to be in the tunneling limit. However, since $\chi = \eta\xi$, these two limits are not independent. It has been shown that in the high-χ limit, the $\xi \to \infty$ and $\chi \to \infty$ limits do not commute [55,56]; here we find ourselves in a similar situation but a different limit. This is essentially due to χ being a compound parameter, depending on the product of particle and field parameter, which are usually considered independently in experiment.

The situation is further complicated by vague language such as "good approximation" and inexact limits like "$\xi \gg 1$, $\chi \ll 1$." In this article we will take a practical approach: we will calculate using the more widely applicable and accurate locally monochromatic approximation (LMA) and compare with the asymptotic tunneling formula in Eq. (1). If the scaling of the pair creation rate with χ and hence with α_{qed} is described by the tunneling formula to within some error (which we nominally take to be 10%), then we conclude in that parameter regime, pair creation exhibits the predicted nonanalytic dependency on α_{qed}. Then the question remains: "how high must ξ be?" and "how small must χ be?" to see this dependency in experiment, i.e., while producing sufficient pairs as to be measurable.

To investigate this, we consider monoenergetic photons with energy parameter η colliding with a plane wave with scaled potential $a = eA$:

$$a(\varphi) = m\xi\varepsilon \sin^2\left(\frac{\varphi}{2N}\right)\cos\varphi \tag{4}$$

for $0 < \varphi < 2\pi N$ where N is the number of cycles and $a(\varphi) = 0$ otherwise, and ε is a linear polarization vector. We can write the ratio of the tunneling and LMA probability as

$$\frac{\mathsf{P}_{\text{tun.}}}{\mathsf{P}_{\text{lma}}} = \frac{\mathsf{P}_{\text{tun.}}}{\mathsf{P}_{\text{lcfa}}} \times \frac{\mathsf{P}_{\text{lcfa}}}{\mathsf{P}_{\text{lma}}}. \tag{5}$$

The first ratio on the right-hand side is a measure of how close the LCFA is to the tunneling regime, and the second ratio is a measure of how close the LCFA is to the LMA and the true probability. We can use this relation to understand when the tunneling regime is arrived at, by plotting in Fig. 1 how close each of these quantities is to unity. (The expressions for P_{lcfa} and P_{lma} can be found in Appendix B.)

In Fig. 1(a) the relative difference of the tunneling formula to the LCFA is plotted, showing when the latter is in the tunneling regime. We note that the accuracy increases in a direction parallel to falling χ, as expected.

In Fig. 1(b), the relative difference of the LMA to the LCFA is plotted. Broadly speaking, there is better agreement when $\xi \gg 1$, but there is a slight tilt with higher energies being more accurate for pair creation.

The main result is in Fig. 1(c). Here we see that if ξ is too small, the tunneling formula is not accurate because the LCFA is not accurate [as reflected by Fig. 1(b)]. Likewise, if the energy is too large, the χ value is too large, and so the tunneling limit is not reached [as reflected by Fig. 1(a)]. Therefore, there is an optimum region in the middle of the plot. For $\eta = 0.1$, we see the region is optimal for the relative difference smaller than 10% for $0.3 \lesssim \chi \lesssim 0.8$, i.e. $3 \lesssim \xi \lesssim 8$, which can correspond to a measurable number of pairs. (In the optimal region, the relative difference between tunneling and LMA probabilities changes sign.)

For a given photon energy, Fig. 1(c) shows the optimal EM background intensity to be in the tunneling regime. However, it is feasible to measure in this regime only if sufficient pairs are generated. In Fig. 2 the "tunneling regime" curve is plotted on top of the probability for pair creation. The optimal parameters for detecting tunneling pair creation can then be seen to be in the "transition regime" of intensity $\xi \gtrsim O(1)$ at higher photon energies $\eta \gtrsim O(0.1)$. It is clear that moving to higher intesities and lower energies, while being in the optimal tunneling regime, will lead to too few pairs being created for experiments, unless they involve a very large number of initial high-energy photons.

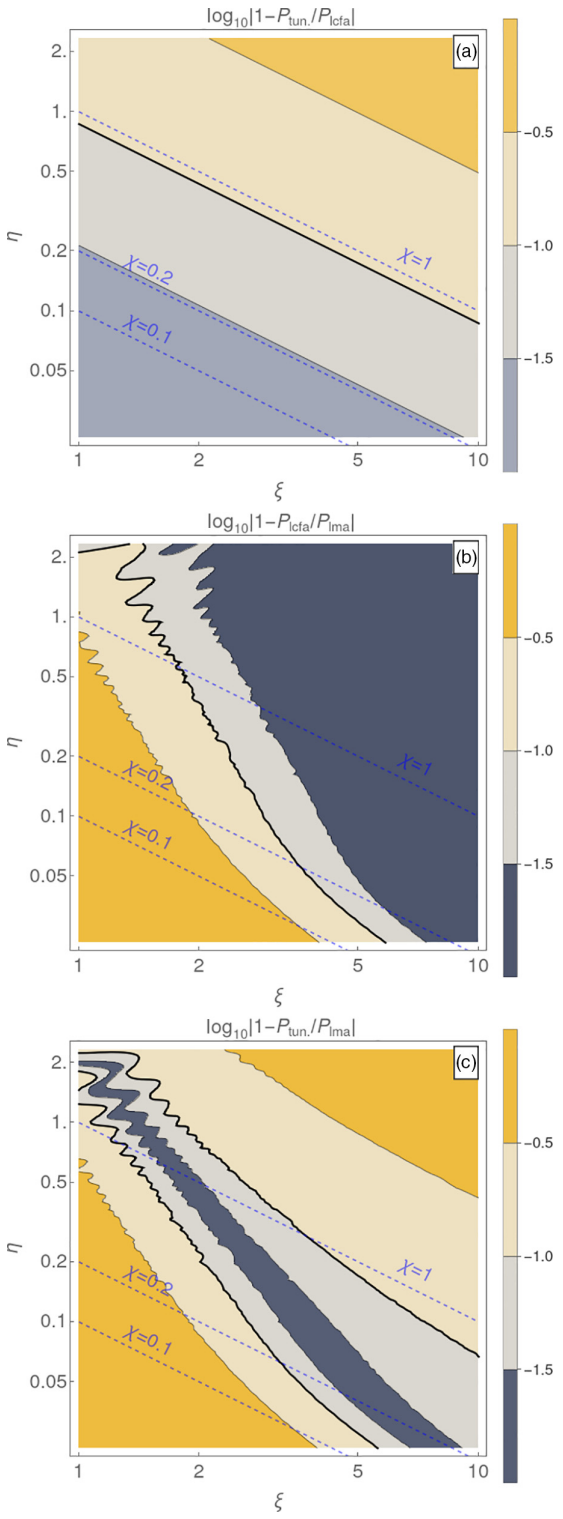

FIG. 1. Relative probabilities for nonlinear Breit-Wheeler pair creation in a four-cycle plane-wave pulse. The thick contour lines denote a relative difference of 10%.

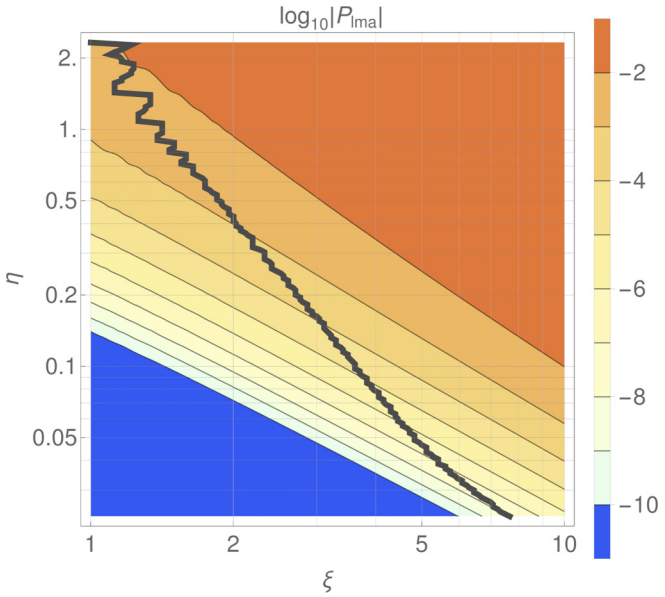

FIG. 2. Probability for pair creation for the monoenergetic photon colliding with a 16-cycle plane-wave. The dark gray line is the "tunneling" region from Fig. 1(c).

III. PHOTON SOURCE

In the cases of photons from bremsstrahlung and inverse Compton sources colliding with a plane wave, there is very little modification of the conclusions in Fig. 1. In the bremsstrahlung case, although the photon spectrum is broad, since pair creation in the tunneling regime depends strongly on the photon energy, the main contribution is just from the highest photon energies. The only difference is in the harmonic structure, which can be seen in the high-η, small-ξ oscillations in the probability in Figs. 1 and 2. For the inverse Compton source, the bandwidth is narrow and quasimonoenergetic. Therefore we move straight to the focused background case.

A. Bremsstrahlung photons

In this section we calculate the probability for pair creation, $\mathsf{P}^{\text{brems}}$, in the collision of thin-target bremsstrahlung with a focused laser pulse [39,40,57,58]. To do this, we integrate the plane-wave probability, P^{pw}, for nonlinear Breit-Wheeler (calculated with the LMA or the tunneling formula) over the impact parameter of the photons in the bremsstrahlung:

$$\mathsf{P}^{\text{brems}} = \int_0^1 ds \int d^2\mathbf{x}^\perp \, \rho_b(s, \mathbf{x}^\perp) \, \mathsf{P}^{\text{pw}}[s, \xi(\mathbf{x}^\perp)], \tag{6}$$

where $\rho_b(s, \mathbf{x}^\perp)$ is a number density of bremsstrahlung photons, $s = \omega_\gamma / p^0$ is the ratio of photon to initial electron beam energy (assumed quasimonoenergetic). The equation in (6) uses a semiclassical approximation assuming that $\gamma \gg \xi^2$ where γ is the created particles' Lorentz gamma factor (see, e.g., [59]). To calculate P we take the example of a paraxial Gaussian beam in the infinite Rayleigh length limit:

$$\xi(\mathbf{x}^\perp) = e^{-\frac{|\mathbf{x}^\perp|^2}{w_0^2}} \xi, \tag{7}$$

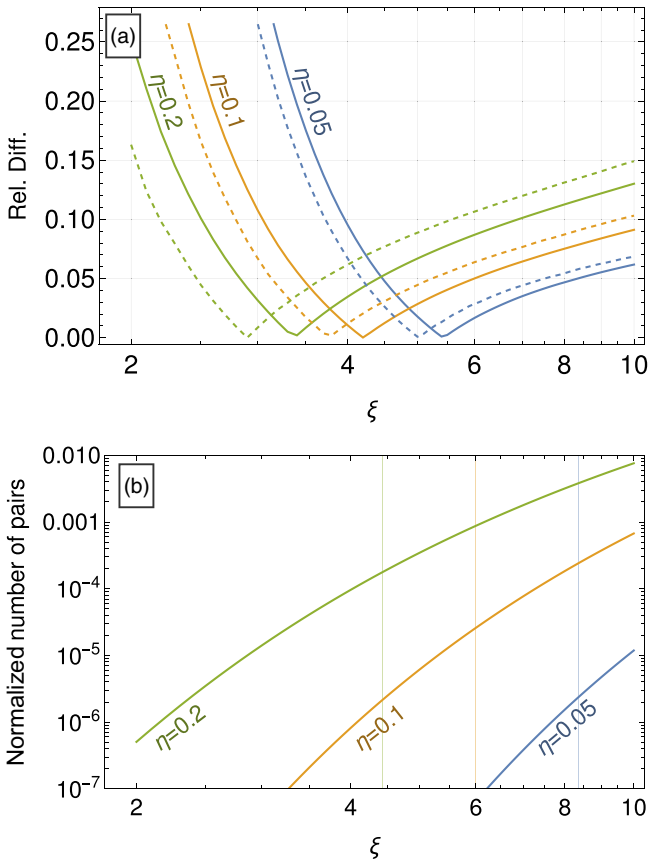

FIG. 3. (a) The relative difference of the tunneling and the LMA calculations. For lines of the same color: the dashed lines are for a plane wave and the solid lines are for the focused Gaussian beam in the infinite Rayleigh length approximation. (b) The normalized number of pairs. The gridlines with the same color as a curve indicate the upper bound of being within 5% of the tunneling formula.

where ξ is the same as in the definition of the plane wave Eq. (4). For the bremsstrahlung, the laser interaction point is typically far enough from the bremsstrahlung source, that over width of the focus of the laser, the bremsstrahlung density can be considered to be independent of transverse coordinate. Then we approximate $\rho_b(s, \mathbf{x}^\perp) \approx \rho_b(s)$ where [60]:

$$\rho_b(s) = \frac{1}{s}\left[\frac{4}{3} - \frac{4}{3}s + s^2\right]. \tag{8}$$

The results of the numerical calculation can be seen in Fig. 3(a), where the vertical axis is the relative difference $|\mathsf{P}^{\text{brems}}_{\text{lma}}/\mathsf{P}^{\text{brems}}_{\text{tun}} - 1|$ where $\mathsf{P}^{\text{brems}}_{\text{lma}}$ ($\mathsf{P}^{\text{brems}}_{\text{tun}}$) is the evaluation of Eq. (6) with the LMA (tunneling formula) for P^{pw}. For the photon energies considered, which are typical for possible laser-particle experiments, the optimal region for measuring tunneling pair creation is approximately in the range $\xi \in [3, 7]$ (for a 20° collision with an optical 800 nm laser pulse, $\eta \in \{0.05, 0.1, 0.2\}$ corresponds to photon energies $\{4.3, 8.7, 17.3\}$ GeV, respectively). However, we also see in Fig. 3(b) that if lower photon energies are considered, for a detectable number of pairs to be generated, the intensities must be increased to the point that $\chi \not\ll 1$ and the process cannot be considered tunneling anymore. This can be seen

by noting what the maximum number of pairs per photon is, for the tunneling formula to be accurate to within 5% as indicated by the vertical gridlines in Fig. 3(b). Although the optimal intensity (and spread of intensities) of the "tunneling" regime increases with decreasing photon energy, the number of pairs produced in this optimal regime falls significantly. For comparison, in the LUXE experiment, with $\eta = 0.192$, the number of bremsstrahlung photons that collide with the laser focus is of the order of 10^5 [14].

B. Inverse Compton source

By combining an electron beam with low energy spread with a weak ($\xi \ll 1$) laser pulse of broad focus, a narrowband source of high-energy photons can be produced via inverse Compton scattering [61–65]. The parameters we choose in this section for the laser pulse and electron beam are motivated by the LUXE experiment [44], for which it is planned to frequency tripling the optical laser and generate a narrowband source of Compton-scattered photons with energies as high as ∼9 GeV.

The inverse Compton source (ICS) can be modeled using the collision between a beam of high-energy electrons (with momentum p^μ) and a weak laser pulse [66], giving the double differential spectrum [67]

$$\frac{d^2\mathsf{P}_\gamma}{ds d\theta} = \frac{\alpha_{\mathsf{qed}}}{(2\pi)^2}\frac{m^2/\omega_l^2 \sin\theta}{(1+\cos\theta)^2}\frac{s}{1-s}\int_{-\pi}^{\pi} d\psi \iint d\varphi_1 d\varphi_2 \times e^{i\int_{\varphi_2}^{\varphi_1}\frac{\ell\cdot\pi_p(\phi)}{m^2\eta_e(1-s)}d\phi}\left[\frac{[a(\varphi_1)-a(\varphi_2)]^2}{2m^2}h_s - 1\right], \quad (9)$$

characterized by the electron energy parameter $\eta_e = \varkappa\cdot p/m^2$ and the intensity ξ of the laser pulse, where $\ell^\mu = \omega_\gamma(1, \sin\theta\cos\psi, \sin\theta\sin\psi, \cos\theta)$ is the momentum of the scattered photon, θ is the angular spread of the scattered photon along the antidirection of the laser pulse, $\varkappa^\mu = \omega_l(1,0,0,-1)$, $s = \varkappa\cdot\ell/\varkappa\cdot p \approx \omega_\gamma/p^0$ for nearly head-on collisions, ω_l is the laser carrier frequency, and $h_s = [1+(1-s)^2]/(2-2s)$, $\pi_p(\phi) = p^\mu + a^\mu - (p\cdot a/\varkappa\cdot p + a^2/2\varkappa\cdot p)\,\varkappa^\mu$ is the instantaneous momentum of the electron.

In Fig. 4 we plot the photon distribution of the ICS scattered from a laser pulse with the sine-squared profile used in Eq. (4). (Since the weak laser is broadly focused, it can be approximated during the interaction with the electron beam to be plane wave in form.) The ICS laser pulse duration is chosen to be FWHM = 25 fs, with carrier frequency (third harmonic) $\omega_l = 4.65$ eV and intensity $\xi = 0.1$, which collides head on with a 16.8 GeV electron, corresponding to the energy parameter $\eta_e = 0.6$. (In the LUXE experiment [14], the electron beam with the energy 16.5 GeV would be applied.) As shown, the ICS photons are quasimonoenergetic in a narrow angular spread $\theta < 10$ μrad, around $s = 2\eta_e/(2\eta_e+1)$ corresponding to the photon energy about $\omega_\gamma = 9.1$ GeV, and the height of the harmonic peaks, around $s = 2n\eta_e/(2n\eta_e+1)$ with the integer $n \geqslant 2$ for the multiphoton scattering, is negligible because of the weak laser intensity.

This ICS photons can be employed to measure tunneling pair creation by colliding with an intense laser pulse downstream the photon beam. The creation yield can be written in

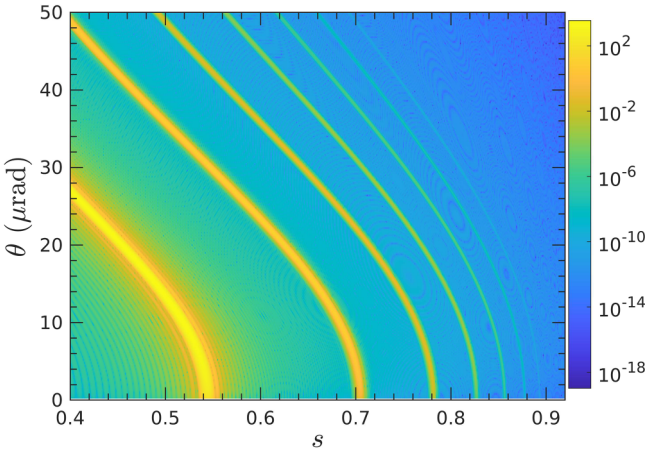

FIG. 4. Double differential spectrum $d^2\mathsf{P}_\gamma/(ds d\theta)$ of the inverse Compton source photons, produced when a 16.8 GeV electron collides head-on with a laser pulse with sine-squared envelope, carrier frequency $\omega_l = 4.65$ eV and intensity $\xi = 0.1$.

form as

$$\mathsf{P}^{\mathsf{ics}} = \iint ds d\theta \,\frac{d^2\mathsf{P}_\gamma}{ds d\theta}\,\mathsf{P}^{\mathsf{pw}}[\omega_\gamma(s), \xi(\theta)], \quad (10)$$

where P^{pw} is the yield of the positrons created by the photon with the energy ω_γ and the scattering angle θ. Again, we consider the infinite Rayleigh length approximation of a Gaussian paraxial beam Eq. (7) with the impact parameter $|\mathbf{x}^\perp| = d\tan\theta$ varying with the scattering angle, and also the intensity $\xi(\theta) = \xi\exp(-d^2\tan^2\theta/w_0^2)$, where $d \sim O(1)$ m is the distance between the ICS and the interaction point with the target Gaussian beam. Figure 5 shows the calculation of

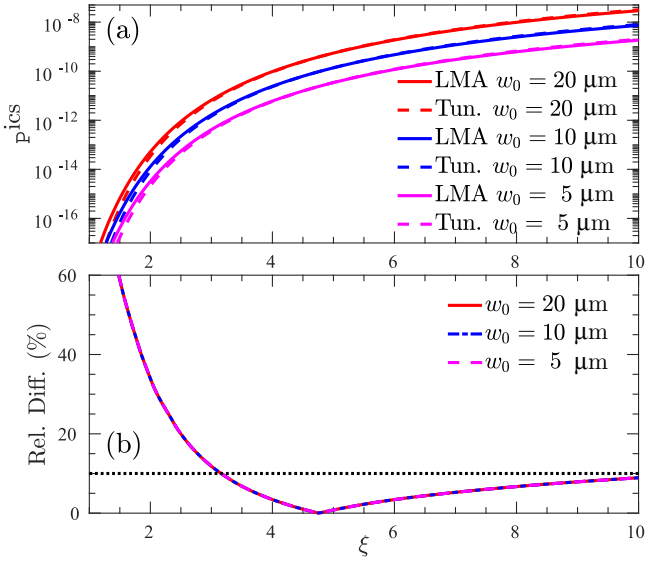

FIG. 5. (a) Positron yield created by the focused pulse with the waist $w_0 = 20$ μm, 10 μm, 5 μm calculated by the LMA and tunneling results. (b) Relative difference between the positron yield calculated with each method: $|\mathsf{P}^{\mathsf{ics}}_{\mathsf{lma}} - \mathsf{P}^{\mathsf{ics}}_{\mathsf{tun}}|/\mathsf{P}^{\mathsf{ics}}_{\mathsf{lma}}$. The black dotted lines denote the relative difference at 10%. The Gaussian pulse has the longitudinal profile (4) with 16 cycles.

the positron yield created by the ICS in Fig. 4 colliding with a Gaussian pulse with the carrier frequency $\omega_l = 1.55$ eV and $d = 7.5$ m downstream, in which the probability of pair creation is calculated with the tunneling rate [Eq. (1)] and the LMA result [Eq. (B2) using the formula in Appendix B], respectively. As shown, the positron yield from the LMA calculation increases rapidly with the increase of the laser intensity in the same trend as that calculated with the tunneling rate, and the relative difference suggests the optimal measurement of the nonanalytic dependency pair creation in the intermediate intensity region around $\xi = 4.5$, similar to the bremsstrahlung case. We find that the transverse waist w_0 of the Gaussian pulse only affects the yield of the positron, but not the optimal intensity regime.

IV. ELECTRON BEAM

The tunneling regime of pair creation can also be accessed via the two-step nonlinear trident process [68–71], in which an electron scatters in a laser pulse to produce a nonlinear Compton scatters which is converted to a pair in the same pulse. The nonlinear trident process thereby combines in the same laser pulse, the photon generation and pair production steps that were separated in the previous section in the bremsstrahlung and ICS setups. Furthermore, the two-step process is expected to dominate the total trident rate when $\xi\omega_l\tau \gg 1$ [51,72–74] (see also [75,76]), which is generally easily fulfilled when intense lasers are employed to search for strong-field QED effects, where τ is the scale of the interaction duration.

The positron yield in the two-step trident process can be simply written as

$$\mathsf{P}^{\mathsf{tri}} = \int_0^1 ds \int_{\varphi_i}^{\varphi_f} d\varphi \frac{d^2\mathsf{P}_\gamma}{ds d\varphi} \int_{\varphi}^{\varphi_f} d\phi \frac{d\mathsf{P}^{\mathsf{pw}}}{d\phi}, \tag{11}$$

where P_γ is the probability of the nonlinear Compton scattering calculated also with the LMA result:

$$\frac{d^2\mathsf{P}_\gamma}{ds d\varphi} = \frac{\alpha_{\mathsf{qed}}}{\eta_e} \sum_{n=\lceil n_c \rceil}^{+\infty} \int_{-\pi}^{\pi} \frac{d\psi}{2\pi} \times \left[\xi^2(\varphi)\left(\Lambda_{1,n}^2 - \Lambda_{0,n}\Lambda_{2,n}\right)h_s - \Lambda_{0,n}^2\right], \tag{12}$$

with $\xi(\varphi) = \xi_0 f(\varphi)$, $\lceil n_c \rceil$ denotes the lowest integer greater than or equal to $n_c = s[1 + \xi^2(\varphi)/2]/[2\eta_e(1-s)]$, $\Lambda_{j,n}(u,v)$ are the generalized Bessel functions defined in Appendix B with $j = 0, 1, 2$ and the arguments given as $u = [r_{c,n} s\xi(\varphi)\cos\psi]/[\eta_e(1-s)]$, $v = s\xi^2(\varphi)/[8\eta_e(1-s)]$, and $r_{c,n} = \sqrt{2n\eta_e(1-s)/s - 1 - \xi^2(\varphi)/2}$. $d\mathsf{P}^{\mathsf{pw}}/d\phi$ is the rate for the pair creation calculated with the tunneling result and the LMA result.

In Fig. 6(a) we show the pair creation via this two-step trident process in a plane wave background triggered by an electron with the parameter $\eta_e = 0.2$, corresponding to the energy of 16.8 GeV. Again, the LMA and the tunneling rate predict the same trend of the pair creation with the increase of the laser intensity. Similar to the cases starting with the photon beam, the numerical comparison in Fig. 6(a) suggests intensities within $2.5 \lesssim \xi \lesssim 7.5$, a "transition regime," for the measurement of this nonanalytic dependency with the relative difference smaller than 10%. For this two-step trident process, the optimal intensity for the smallest difference becomes slightly lower than $\xi = 4$. This is because the dominant contribution for the pair creation comes from the intermediate photon with the energy $\eta = 0.6\eta_e = 0.12$ [71], slightly larger than that in Fig. 5.

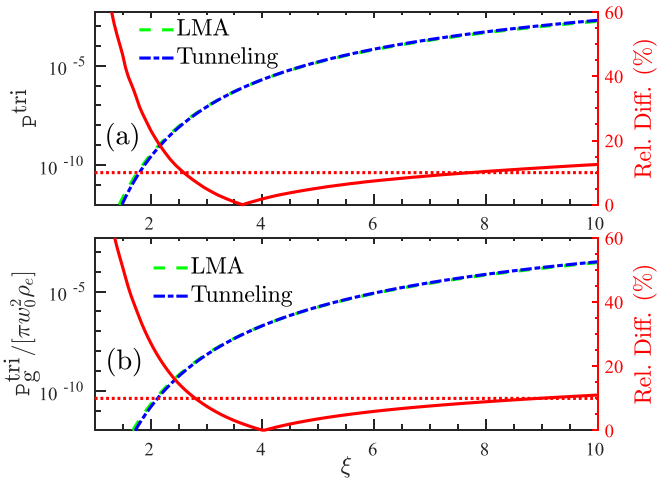

FIG. 6. Positron yield created in a plane wave (a) and a Gaussian beam (b) with 16 cycles and intensity ξ calculated by the LMA and tunneling results. The relative difference (red solid line) between the two methods $|\mathsf{P}^{\mathsf{tri}}_{\mathsf{lma}} - \mathsf{P}^{\mathsf{tri}}_{\mathsf{tun}}|/\mathsf{P}^{\mathsf{tri}}_{\mathsf{lma}}$ is shown with the right vertical axis in each panel, and the red dotted lines denote the relative difference at 10%.

In Fig. 6(b) we consider this two-step trident pair creation in the Gaussian beam [Eq. (7)] downstream of the electron beam, in which we assume that the electron transverse scale is much broader than that of the Gaussian beam and can thus write the total pair creation by integrating the plane-wave results over the impact parameter of the laser beam

$$\mathsf{P}_{\mathsf{g}}^{\mathsf{tri}} = \iint d^2\boldsymbol{x}^\perp \rho_e(\boldsymbol{x}^\perp)\mathsf{P}^{\mathsf{tri}}[\xi(\mathbf{x}^\perp)] \approx \pi w_0^2 \rho_e \int_0^\infty dx\, \mathsf{P}^{\mathsf{tri}}[e^{-x}\xi], \tag{13}$$

where ρ_e is number density of the electron beam. Similar to the plane-wave results in Fig. 6(a), the trident pair creation in the Gaussian beam also suggests a similar "transition regime" of the intensity $3.0 \lesssim \xi \lesssim 8.0$ as the optimal regime for the measurement of the tunneling pair creation. The trident results are particularly significant because the probability for pair creation in the tunneling regime is in general quite low, and producing pairs in the pulse rather than separating the photon-generation and production mechanisms is more efficient.

V. CONCLUSION

One of the interesting aspects of strong-field quantum electrodynamics in laser pulses is that exact solutions to the Dirac equation can be used to show a dependency on the coupling that cannot be arrived at using standard tools of perturbation theory. There are two "nonperturbative" dependencies: (1) an all-order dependence on the charge-field coupling, ξ when $\xi \ll 1$ (a classical effect) and (2) a nonanalytic dependence on the fundamental coupling, α_{qed} in the quasistatic regime

(a quantum effect). The relevant parameter in experiments that collide laser pulses with particle beams is the strong-field parameter, $\chi \propto \sqrt{\alpha_{\mathsf{qed}}}$. It was recently reported that the nonanalytic dependency can be revealed also in nonlinear Compton scattering by making a suitable cut in the transverse momentum spectrum [77,78] (a similar dependency was also noted in [79]); here we focused on accessing the nonanalytic scaling in experiments measuring the tunneling regime of nonlinear Breit-Wheeler pair creation from a photon for which $\chi \ll 1$. Our analysis assumes that in the tunneling regime, a plane-wave approximation is still accurate to describe pair creation in focused laser pulses. Because the tunneling exponent is sensitive to the exact field invariants of a given scenario, we should expect that our results apply to weakly focused laser pulses. Although such laser pulses have a lower peak intensity than in the strongly focused case, they are useful in experiment as they provide broader focal spots and hence minimize variation due to pulse and beam jitter. To reach the corresponding tunneling regime, the intensity parameter must be large enough to be in the quasistatic regime (where the locally constant field approximation [51,80–82] applies), but not too large that $\chi \ll 1$, while also producing sufficient pairs to be measurable in experiment. To assess for which parameter regime measuring the nonanalytic dependency is feasible, we employed the locally monochromatic approximation, which allows one to determine (1) when the process is in the quasistatic regime and (2) when the tunneling limit of the quasistatic regime has been reached. This allowed us to identify a regime that was relatively consistent throughout scenarios where bremsstrahlung and inverse Compton sources of photons collided with focused laser pulses as well as in scenarios where pair creation proceeded directly in the laser pulse in an electron beam-laser collision. For photon energies of $\sim O(10\,\mathrm{GeV})$ the regime of intensity parameter, ξ, should ideally be in the intermediate intensity regime $3 \lesssim \xi \lesssim 8$, corresponding to $\chi \approx 0.5$. Lower photon energies may be used by raising the intensity parameter, but at the cost of reducing the number of pairs. The optimal parameter region can be accessed at laser-particle experiments such as LUXE and E320 and also in the most recent high-intensity laser facilities [16].

ACKNOWLEDGMENTS

The authors thank Tom Blackburn for providing useful data from the Ptarmigan rate generator. The authors also thank the organizers of the "LUXE physics and SFQED" workshop at the Weizmann Institute, where the idea for this paper was generated. S.T. acknowledges the support from the Natural Science Foundation of China, Grant No. 12104428. The work was carried out in part at Marine Big Data Center of Institute for Advanced Ocean Study of Ocean University of China.

APPENDIX A: FIELD INVARIANTS IN NONLINEAR BREIT-WHEELER

Consider the collision of a weak EM probe, f_p with an intense background, F_{bg}. Then the total field is

$$F = F_{\mathsf{bg}} + f_p.$$

In studies of the Breit-Wheeler process, F_{bg} is usually a plane wave, or a perturbation away from it (e.g., a weakly focused Gaussian beam). In studies of the Schwinger process, F_{bg} is a constant or slowly varying but homogeneous electric field and $f_p = 0$ or else f_p is a high-frequency field and one writes of "assisted Schwinger." Breit-Wheeler is then distinguished from Schwinger on the basis of F_{bg} being a plane wave, and hence the invariants $\mathcal{S}_{\mathsf{bg}} = -F_{\mathsf{bg}} \cdot F_{\mathsf{bg}}/4$ and $\mathcal{P}_{\mathsf{bg}} = -F_{\mathsf{bg}} \cdot \widetilde{F}_{\mathsf{bg}}/4$ being zero. A fairer comparison would be to calculate the invariant of the full field. Writing the plane-wave background and probe as

$$\begin{aligned} F_{\mathsf{bg}} &= m\xi_{\mathsf{bg}}[\varkappa^\mu \epsilon^\nu - \varkappa^\nu \epsilon^\mu], \\ f_{p,j} &= m\xi_p\left[\ell^\mu \varepsilon_j^\nu - \ell^\nu \varepsilon_j^\mu\right] \end{aligned} \tag{A1}$$

and choosing the light-front polarization basis as $\varepsilon_j = \epsilon_j - \varkappa \ell \cdot \epsilon_j/\varkappa \cdot \ell$, with $\epsilon_1 = \epsilon$ and ϵ_2 a spacelike vector perpendicular to $\varkappa$ and ϵ_1, we see

$$\begin{aligned} \mathcal{S} &= -\tfrac{1}{4} F \cdot F = F_{\mathsf{qed}}^2 \xi_p \chi\ \delta_{j1}, \\ \mathcal{P} &= -\tfrac{1}{4} F \cdot \widetilde{F} = F_{\mathsf{qed}}^2 \xi_p \chi\ \delta_{j2}, \end{aligned}$$

where δ_{jk} refers to the polarization state of the probe, the strong-field parameter is $\chi = \xi_{\mathsf{bg}}\eta$, the energy parameter is $\eta = \varkappa \cdot \ell/m^2$, and the QED strong field scale (sometimes referred to as the "Schwinger limit") is $F_{\mathsf{qed}} = m^2/e$. At high background field intensities $\xi_{\mathsf{bg}} \gg 1$, it is known that the Breit-Wheeler probabilities are well characterized by a "locally constant" rate, which depends nontrivially only on the strong-field parameter χ. Hence far from being zero for Breit-Wheeler, the EM invariants are proportional to the strong-field parameter.

APPENDIX B: LMA AND LCFA FOR NONLINEAR BREIT-WHEELER

Here we list the formulas used in the main text for nonlinear Breit-Wheeler pair creation. (The derivation of these forms can be found in [83].)

The LCFA probability rate can be written as

$$\frac{d\mathsf{P}_{\mathsf{lcfa}}}{d\varphi} = \frac{\alpha_{\mathsf{qed}}}{\eta} \int_0^1 dt \left[\mathrm{Ai}_1(z) - \mathrm{Ai}'(z) \frac{s^2 + (1-t)^2}{t(1-t)z} \right], \tag{B1}$$

where the argument of the Airy functions is given as $z = [s(1-s)\eta|\xi(\varphi)|]^{-2/3}$, and $t = \varkappa \cdot q/\varkappa \cdot \ell$ is the fraction of the light-front momentum taken by the positron from the incoming photon, and $t \approx E_q/\omega_\gamma$ approximates as the energy ratio for nearly head-on collisions.

In linearly polarized laser backgrounds, the LMA probability rate is expressed as

$$\begin{aligned} \frac{d\mathsf{P}_{\mathsf{lma}}}{d\varphi} = \frac{\alpha_{\mathsf{qed}}}{\eta} \int_0^1 dt \int_{-\pi}^{\pi} \frac{d\psi}{2\pi} \sum_{n=\lceil n_* \rceil} \\ \times \left[\xi^2(\varphi)\left(\Lambda_{1,n}^2 - \Lambda_{0,n}\Lambda_{2,n}\right) \frac{t^2 + (1-t^2)}{2t(1-t)} + \Lambda_{0,n}^2 \right], \end{aligned} \tag{B2}$$

where $n_* = [1+\xi^2(\varphi)/2]/[2\eta(1-t)t]$, $\Lambda_{j,n}(\zeta,\beta)$ is the generalized Bessel functions defined as

$$\Lambda_{j,n}(\zeta,\beta) = \int_{-\pi}^{\pi} \frac{d\phi}{2\pi} \cos^j(\phi) e^{i[n\phi - \zeta\,\sin(\phi)+\beta\,\sin(2\phi)]},$$

with $j = 0, 1, 2,$ and the arguments $\zeta = [\xi(\varphi) r_{b,n} \cos\psi]/[\eta t(1-t)]$, $\beta = \xi^2(\varphi)/[8\eta t(1-t)]$, and $r_{b,n} = \sqrt{2n\eta(1-t)t - 1 - \xi^2(\varphi)/2}$.

[1] G. Breit and J. A. Wheeler, Collision of two light quanta, Phys. Rev. **46**, 1087 (1934).

[2] M. Aaboud *et al.* (ATLAS Collaboration), Evidence for light-by-light scattering in heavy-ion collisions with the ATLAS detector at the LHC, Nat. Phys. **13**, 852 (2017).

[3] G. Aad *et al.* (ATLAS Collaboration), Observation of light-by-light scattering in ultraperipheral Pb + Pb collisions with the ATLAS detector, Phys. Rev. Lett. **123**, 052001 (2019).

[4] A. M. Sirunyan *et al.* (CMS Collaboration), Evidence for light-by-light scattering and searches for axion-like particles in ultraperipheral PbPb collisions at $\sqrt{s_{\rm NN}} = 5.02$ TeV, Phys. Lett. B **797**, 134826 (2019).

[5] H. Bethe and W. Heitler, On the stopping of fast particles and on the creation of positive electrons, Proc. R. Soc. London A **146**, 83 (1934).

[6] H. R. Reiss, Absorption of light by light, J. Math. Phys. **3**, 59 (1962).

[7] A. I. Nikishov and V. I. Ritus, Quantum processes in the field of a plane electromagnetic wave and in a constant field 1, Sov. Phys. JETP **19**, 529 (1964) [Zh. Eksp. Teor. Fiz. **46**, 776(1964)].

[8] T. Heinzl, A. Ilderton, and M. Marklund, Finite size effects in stimulated laser pair production, Phys. Lett. B **692**, 250 (2010).

[9] T. Nousch, D. Seipt, B. Kampfer, and A. I. Titov, Pair production in short laser pulses near threshold, Phys. Lett. B **715**, 246 (2012).

[10] K. Krajewska and J. Z. Kaminski, Breit-wheeler process in intense short laser pulses, Phys. Rev. A **86**, 052104 (2012).

[11] S. Meuren, C. H. Keitel, and A. Di Piazza, Semiclassical picture for electron-positron photoproduction in strong laser fields, Phys. Rev. D **93**, 085028 (2016).

[12] D. L. Burke, R. C. Field, G. Horton-Smith, J. E. Spencer, D. Walz, S. C. Berridge, W. M. Bugg, K. Shmakov, A. W. Weidemann, C. Bula *et al.*, Positron production in multiphoton light-by-light scattering, Phys. Rev. Lett. **79**, 1626 (1997).

[13] C. Bamber, S. J. Boege, T. Koffas, T. Kotseroglou, A. C. Melissinos, D. D. Meyerhofer, D. A. Reis, W. Ragg, C. Bula, K. T. McDonald *et al.*, Studies of nonlinear QED in collisions of 46.6 GeV electrons with intense laser pulses, Phys. Rev. D **60**, 092004 (1999).

[14] H. Abramowicz, U. Acosta, M. Altarelli, R. Aßmann, Z. Bai, T. Behnke, Y. Benhammou, T. Blackburn, S. Boogert, O. Borysov *et al.*, Conceptual design report for the LUXE experiment, Eur. Phys. J. Spec. Top. **230**, 2445 (2021).

[15] Z. Chen, S. Meuren, E. Gerstmayr, V. Yakimenko, P. H. Bucksbaum, and D. A. Reis, Preparation of strong-field QED experiments at facet-II, in *Optica High-Brightness Sources and Light-Driven Interactions Congress 2022* (Optica Publishing Group, Budapest, Hungary, 2022), p. HF4B.6.

[16] C. N. Danson, C. Haefner, J. Bromage, T. Butcher, J.-C. F. Chanteloup, E. A. Chowdhury, A. Galvanauskas, L. A. Gizzi, J. Hein, D. I. Hillier *et al.*, Petawatt and exawatt class lasers worldwide, High Power Laser Sci. Eng. **7**, e54 (2019).

[17] H. Abramowicz *et al.*, Letter of intent for the LUXE experiment, arXiv:1909.00860..

[18] L. V. Gribov, E. M. Levin, and M. G. Ryskin, Semihard processes in QCD, Phys. Rep. **100**, 1 (1983).

[19] M. S. Abdallah *et al.* (STAR Collaboration), Evidence for nonlinear gluon effects in QCD and their mass number dependence at STAR, Phys. Rev. Lett. **129**, 092501 (2022).

[20] J. S. Schwinger, On gauge invariance and vacuum polarization, Phys. Rev. **82**, 664 (1951).

[21] F. Sauter, Uber das Verhalten eines Elektrons im homogenen elektrischen Feld nach der relativistischen Theorie Diracs, Z. Phys. **69**, 742 (1931).

[22] W. Heisenberg and H. Euler, Folgerungen aus der Diracschen Theorie des Positrons, Z. Phys. **98**, 714 (1936).

[23] R. Schützhold, H. Gies, and G. Dunne, Dynamically assisted Schwinger mechanism, Phys. Rev. Lett. **101**, 130404 (2008).

[24] M. Orthaber, F. Hebenstreit, and R. Alkofer, Momentum spectra for dynamically assisted Schwinger pair production, Phys. Lett. B **698**, 80 (2011).

[25] F. Hebenstreit, R. Alkofer, and H. Gies, Particle self-bunching in the Schwinger effect in spacetime-dependent electric fields, Phys. Rev. Lett. **107**, 180403 (2011).

[26] C. Kohlfürst, M. Mitter, G. von Winckel, F. Hebenstreit, and R. Alkofer, Optimizing the pulse shape for Schwinger pair production, Phys. Rev. D **88**, 045028 (2013).

[27] C. Schneider and R. Schützhold, Dynamically assisted Sauter-Schwinger effect in inhomogeneous electric fields, J. High Energy Phys. 02 (2016) 164.

[28] G. Torgrimsson, J. Oertel, and R. Schützhold, Doubly assisted Sauter-Schwinger effect, Phys. Rev. D **94**, 065035 (2016).

[29] G. Torgrimsson, C. Schneider, and R. Schützhold, Sauter-Schwinger pair creation dynamically assisted by a plane wave, Phys. Rev. D **97**, 096004 (2018).

[30] I. A. Aleksandrov, G. Plunien, and V. M. Shabaev, Dynamically assisted Schwinger effect beyond the spatially-uniform-field approximation, Phys. Rev. D **97**, 116001 (2018).

[31] B. S. Xie, Z. L. Li, and S. Tang, Electron-positron pair production in ultrastrong laser fields, Matter Radiat. Extremes **2**, 225 (2017).

[32] O. Olugh, Z. Li, and B. Xie, Dynamically assisted pair production for various polarizations, Phys. Lett. B **802**, 135259 (2020).

[33] L.-J. Li, M. Mohamedsedik, and B.-S. Xie, Enhanced dynamically assisted pair production in spatial inhomogeneous electric fields with the frequency chirping, Phys. Rev. D **104**, 036015 (2021).

[34] A. Ilderton, Physics of adiabatic particle number in the Schwinger effect, Phys. Rev. D **105**, 016021 (2022).

[35] I. Akal, S. Villalba-Chávez, and C. Müller, Electron-positron pair production in a bifrequent oscillating electric field, Phys. Rev. D **90**, 113004 (2014).

[36] J. Braß, R. Milbradt, S. Villalba-Chávez, G. G. Paulus, and C. Müller, Two-color phase-of-the-phase spectroscopy applied to nonperturbative electron-positron pair production in strong oscillating electric fields, Phys. Rev. A **101**, 043401 (2020).

[37] N. Folkerts, J. Putzer, S. Villalba-Chávez, and C. Müller, Electron-positron-pair creation in the superposition of two oscillating electric-field pulses with largely different frequency, duration, and relative positioning, Phys. Rev. A **107**, 052210 (2023).

[38] N. Mahlin, S. Villalba-Chávez, and C. Müller, Dynamically assisted nonlinear Breit-Wheeler pair production in bichromatic laser fields of circular polarization, Phys. Rev. D **108**, 096023 (2023).

[39] H. R. Reiss, Production of electron pairs from a zero-mass state, Phys. Rev. Lett. **26**, 1072 (1971).

[40] A. Hartin, A. Ringwald, and N. Tapia, Measuring the boiling point of the vacuum of quantum electrodynamics, Phys. Rev. D **99**, 036008 (2019).

[41] D. Papadopoulos, J. Zou, C. Le Blanc, G. Chériaux, P. Georges, F. Druon, G. Mennerat, P. Ramirez, L. Martin, A. Fréneaux *et al.*, The Apollon 10 PW laser: experimental and theoretical investigation of the temporal characteristics, High Power Laser Sci. Eng. **4**, e34 (2016).

[42] J. H. Sung, H. W. Lee, J. Y. Yoo, J. W. Yoon, C. W. Lee, J. M. Yang, Y. J. Son, Y. H. Jang, S. K. Lee, and C. H. Nam, 4.2 PW, 20 fs Ti:sapphire laser at 0.1 Hz, Opt. Lett. **42**, 2058 (2017).

[43] S. Weber, S. Bechet, S. Borneis, L. Brabec, M. Bučka, E. Chacon-Golcher, M. Ciappina, M. DeMarco, A. Fajstavr, K. Falk *et al.*, P3: An installation for high-energy density plasma physics and ultra-high intensity laser–matter interaction at ELI-Beamlines, Matter Radiat. Extremes **2**, 149 (2017).

[44] H. Abramowicz *et al.*, Technical design report for the LUXE experiment, arXiv:2308.00515.

[45] T. Heinzl, B. King, and A. J. MacLeod, The locally monochromatic approximation to QED in intense laser fields, Phys. Rev. A **102**, 063110 (2020).

[46] T. G. Blackburn and B. King, Higher fidelity simulations of nonlinear Breit–Wheeler pair creation in intense laser pulses, Eur. Phys. J. C **82**, 44 (2022).

[47] S. Tang and B. King, Pulse envelope effects in nonlinear Breit-Wheeler pair creation, Phys. Rev. D **104**, 096019 (2021).

[48] T. G. Blackburn, B. King, and S. Tang, Simulations of laser-driven strong-field QED with Ptarmigan: Resolving wavelength-scale interference and γ-ray polarization, Phys. Plasmas **30**, 093903 (2023).

[49] T. G. Blackburn, Ptarmigan, github.com/tgblackburn/ptarmigan (2023).

[50] G. Torgrimsson, Loops and polarization in strong-field QED, New J. Phys. **23**, 065001 (2021).

[51] V. I. Ritus, Quantum effects of the interaction of elementary particles with an intense electromagnetic field, J. Russ. Laser Res. **6**, 497 (1985).

[52] A. I. Nikishov, Pair production by a constant external field, Zk. Eksp. Teor. Fiz. **30**, 660 (1969).

[53] N. Narozhny, S. Bulanov, V. Mur, and V. Popov, e^+e^- pair production by a focused laser pulse in vacuum, Phys. Lett. A **330**, 1 (2004).

[54] A. M. Fedotov, Electron-positron pair creation by a strong tightly focused laser field, Laser Phys. **19**, 214 (2009).

[55] A. Ilderton, Note on the conjectured breakdown of QED perturbation theory in strong fields, Phys. Rev. D **99**, 085002 (2019).

[56] T. Podszus and A. Di Piazza, High-energy behavior of strong-field QED in an intense plane wave, Phys. Rev. D **99**, 076004 (2019).

[57] T. G. Blackburn and M. Marklund, Nonlinear Breit-Wheeler pair creation with bremsstrahlung γ rays, Plasma Phys. Control. Fusion **60**, 054009 (2018).

[58] A. Golub, S. Villalba-Chávez, and C. Müller, Nonlinear Breit-Wheeler pair production in collisions of bremsstrahlung γ quanta and a tightly focused laser pulse, Phys. Rev. D **105**, 116016 (2022).

[59] A. Di Piazza, Nonlinear Breit-Wheeler pair production in a tightly focused laser beam, Phys. Rev. Lett. **117**, 213201 (2016).

[60] Y.-S. Tsai, Pair production and bremsstrahlung of charged leptons, Rev. Mod. Phys. **46**, 815 (1974).

[61] K. Aoki, K Hosono, T. Hadame, H. Munenaga, K. Kinoshita, M. Toda, S. Amano, S. Miyamoto, T. Mochizuki, M. Aoki *et al.*, High-energy photon beam production with laser-Compton backscattering, Nucl. Instrum. Methods Phys. Res. A **516**, 228 (2004).

[62] H. R. Weller, M. W. Ahmed, H. Gao, W. Tornow, Y. K. Wu, M. Gai, and R. Miskimen, Research opportunities at the upgraded HIγS facility, Prog. Part. Nucl. Phys. **62**, 257 (2009).

[63] F. Albert, S. G. Anderson, D. J. Gibson, C. A. Hagmann, M. S. Johnson, M. Messerly, V. Semenov, M. Y. Shverdin, B. Rusnak, A. M. Tremaine *et al.*, Characterization and applications of a tunable, laser-based, MeV-class Compton-scattering γ-ray source, Phys. Rev. ST Accel. Beams **13**, 070704 (2010).

[64] S. G. Rykovanov, C. G. R. Geddes, J. L. Vay, C. B. Schroeder, E. Esarey, and W. P. Leemans, Quasi-monoenergetic femtosecond photon sources from Thomson scattering using laser plasma accelerators and plasma channels, J. Phys. B: At. Mol. Opt. Phys. **47**, 234013 (2014).

[65] D. Seipt, S. G. Rykovanov, A. Surzhykov, and S. Fritzsche, Narrowband inverse Compton scattering x-ray sources at high laser intensities, Phys. Rev. A **91**, 033402 (2015).

[66] G. A. Krafft, B. Terzić, E. Johnson, and G. Wilson, Scattered spectra from inverse Compton sources operating at high laser fields and high electron energies, Phys. Rev. Accel. Beams **26**, 034401 (2023).

[67] B. King and S. Tang, Nonlinear compton scattering of polarized photons in plane-wave backgrounds, Phys. Rev. A **102**, 022809 (2020).

[68] V. Dinu and G. Torgrimsson, Approximating higher-order nonlinear QED processes with first-order building blocks, Phys. Rev. D **102**, 016018 (2020).

[69] V. Dinu and G. Torgrimsson, Trident process in laser pulses, Phys. Rev. D **101**, 056017 (2020).

[70] A. I. Titov, U. H. Acosta, and B. Kampfer, Positron energy distribution in a factorized trident process, Phys. Rev. A **104**, 062811 (2021).

[71] S. Tang and B. King, Locally monochromatic two-step nonlinear trident process in a plane wave, Phys. Rev. D **107**, 096004 (2023).

[72] B. King and H. Ruhl, Trident pair production in a constant crossed field, Phys. Rev. D **88**, 013005 (2013).

[73] V. Dinu and G. Torgrimsson, Trident pair production in plane waves: Coherence, exchange, and spacetime inhomogeneity, Phys. Rev. D **97**, 036021 (2018).

[74] F. Mackenroth and A. Di Piazza, Nonlinear trident pair production in an arbitrary plane wave: A focus on the properties of the transition amplitude, Phys. Rev. D **98**, 116002 (2018).

[75] H. Hu, C. Muller, and C. H. Keitel, Complete QED theory of multiphoton trident pair production in strong laser fields, Phys. Rev. Lett. **105**, 080401 (2010).

[76] A. Ilderton, Trident pair production in strong laser pulses, Phys. Rev. Lett. **106**, 020404 (2011).

[77] B. Kämpfer and A. I. Titov, Impact of laser polarization on q-exponential photon tails in non-linear Compton scattering, Phys. Rev. A **103**, 033101 (2021).

[78] U. H. Acosta, A. I. Titov, and B. Kämpfer, Rise and fall of laser-intensity effects in spectrally resolved Compton process, New J. Phys. **23**, 095008 (2021).

[79] V. Dinu and G. Torgrimsson, Single and double nonlinear Compton scattering, Phys. Rev. D **99**, 096018 (2019).

[80] C. N. Harvey, A. Ilderton, and B. King, Testing numerical implementations of strong field electrodynamics, Phys. Rev. A **91**, 013822 (2015).

[81] A. Di Piazza, M. Tamburini, S. Meuren, and C. H. Keitel, Implementing nonlinear Compton scattering beyond the local constant field approximation, Phys. Rev. A **98**, 012134 (2018).

[82] D. Seipt and B. King, Spin- and polarization-dependent locally-constant-field-approximation rates for nonlinear Compton and Breit-Wheeler processes, Phys. Rev. A **102**, 052805 (2020).

[83] S. Tang, Fully polarized nonlinear Breit-Wheeler pair production in pulsed plane waves, Phys. Rev. D **105**, 056018 (2022).